Hurricane Georges's Landfall in the Dominican Republic: Detailed Airborne Doppler Radar Imagery

Bart Geerts,* Gerald M. Heymsfield,* Lin Tian,* Jeffrey B. Halverson,*
Anthony Guillory,+ and Mercedes I. Mejia#

ABSTRACT

Current understanding of landfalling tropical cyclones is limited, especially with regard to convective-scale processes. On 22 September 1998 Hurricane Georges made landfall on the island of Hispaniola, leaving behind a trail of death and devastation, largely the result of excessive rainfall, not storm surge or wind. Detailed airborne measurements were taken as part of the Third Convection and Moisture Experiment. Of particular interest are the ER-2 nadir X-band Doppler radar data, which provide a first-time, high-resolution view of the precipitation and airflow changes as a hurricane interacts with mountainous terrain.

The circulation of Hurricane Georges obviously declined during landfall, evident in the rapid increase in minimum sea level pressure, the subsidence of the eyewall anvil, and the decrease in average ice concentrations in the eyewall. The eye, as seen in satellite imagery, disappeared as deep convection erupted *within* the eye. The main convective event within the eye, with upper-level updraft magnitudes over 20 m s^{-1} and microwave brightness temperatures below 100 K at 89 GHz (implying large ice concentrations), occurred when the eye moved over the Cordillera Central, the island's main mountain chain. The location, intensity and evolution of this convection indicate that it was coupled to the surface orography. The authors speculate that orographic lifting released potential energy, which had been trapped beneath the eye's subsidence inversion.

It is likely that surface rain rates increased during landfall, both in the convective and in the more widespread stratiform rainfall areas over the island. Evidence for this is the increase in radar reflectivity below the bright band down to ground level. Such increase was absent offshore. This low-level rain enhancement must be due to the ascent of boundary layer air over the topography.

1. Introduction

Hurricanes, especially landfalling ones, have been identified as one of four key topics of focus in the United States Weather Research Program (USWRP) for the next five years (2000–04).[1] A second key topic is quantitative precipitation estimation, for which there is a special interest in the case of landfalling hurricanes. The USWRP Fifth Prospectus Development Team (FPDT) identified six key research objectives in the quest to better understand and forecast landfalling tropical cyclones (Marks et al. 1998). One of these is an improved analysis and prediction of surface rainfall. The aftermaths of Hurricanes Mitch (1998) in Honduras and Nicaragua (Ferraro et al. 1999), and Floyd (1999) in North Carolina, provide an even stronger incentive to improve observations and forecasts of rainfall intensities and totals, in addition to surface winds. Another key research objective of the USWRP FPDT relates to severe weather, which includes questions about the likelihood and dynamic significance of convective cells overshooting the anvil top ("hot towers"; Simpson et al. 1998) in landfalling hurricanes. Tropical cyclones are of increasing concern also in East Asia. For instance, in May 1997 a workshop was conducted on typhoon research in the Taiwan area

[1]Available online at http://uswrp.mmm.ucar.edu/uswrp.html.

*NASA Goddard Space Flight Center, Greenbelt, Maryland.
+NASA Marshall Space Flight Center, Huntsville, Alabama.
#Oficina Nacional de Meteorologia, Santa Domingo, Dominican, Republic.
Corresponding author address: Dr. Bart Geerts, Department of Atmospheric Sciences, University of Wyoming, Laramie, WY 82071-3038.
E-mail: geerts@uwyo.edu
In final form 27 November 1999.

(Wu and Kuo 1999). This workshop considered mesoscale convective systems embedded in tropical cyclones, and the rainfall they produce, as one of three key topics of future research. The two other priorities listed relate to the effect of Taiwan's topography and to operational prediction.

Clearly research interest in landfalling tropical cyclones has surged. The Hurricane Research Division (HRD) of the National Oceanic and Atmospheric Administration (NOAA) now collects airborne Doppler radar observations and dropsonde data for every landfalling Atlantic hurricane (e.g., Marks and Houze 1987; Black and Willoughby 1992; Black et al. 1996; Dodge et al. 1999a). This paper focuses on convective-scale changes in the circulation of a hurricane as it makes landfall on complex terrain. Not much is known about this. The subsidence in the center of a hurricane is a dynamic response to latent heating in the eyewall and is responsible for the absence of clouds in the eye. One or more well-defined subsidence inversions may exist in the eye, separating dry air aloft from air with a high θ_e (equivalent potential temperature) below (Willoughby 1998). The eyewall and eye are heated by latent heat release and subsidence, respectively, and the amount of heating is proportional to the sea level pressure (SLP) deficit (through hydrostatic balance), so the minimum SLP is a good measure of storm intensity. The radii of the eyewall and that of the maximum wind tend to shrink in response to circularly symmetric convective heating, and such contraction is opposed by surface friction (Shapiro and Willoughby 1982; Willoughby 1990; Willoughby et al. 1982). A weak inner eyewall is sometimes replaced by an outer one, which moves inward in response to enhanced convection (Willoughby et al. 1982; Black and Willoughby 1992). Latent heat fluxes over warm water increase rapidly with increasing wind speed, making a hurricane an effective heat engine (Emmanuel 1986). Upon landfall these fluxes shut down, the eyewall convection quickly diminishes, and frictional dissipation combines with barotropic instability to decrease the storm's kinetic energy. Frictional convergence and the ceasing of forced eye subsidence cause the eye to become filled with clouds and precipitation. Orography would cause eyewall convection to become asymmetric, much in the same way as environmental shear does, and some convectively generated energy would have to be used toward the forcing of asymmetric motions. Therefore landfall over complex terrain would lead to more rapid dissipation of the storm's circulation.

This paper aims to document changes in Hurricane Georges's cloud and precipitation morphology as it makes landfall on Hispaniola. Following a brief summary of some recent literature on landfalling hurricanes (section 2), surface observations and aircraft operations will be discussed in sections 3 and 4. *Geostationary Operational Environmental Satellite-8* (*GOES-8*) imagery, satellite microwave data, and ground-based radar reflectivity data serve to depict the evolution in a broad temporal and spatial window (section 5), but the focus is on ER-2 nadir X-band Doppler radar (EDOP) nadir reflectivity and velocity cross sections of some spectacular convection (section 6). These observations will then be used to interpret the eye-filling process as well as changes in the eyewall, in particular with regard to reflectivity profiles and surface rainfall (section 7).

2. Landfalling hurricanes: Some previous work

Very few observational studies have focused on the convective scale of landfalling hurricanes. The landmark study by Marks and Houze (1987) documents the reflectivity and airflow of Hurricane Alicia's inner core, while Alicia was still about 90 km from the Texas coast. Ground-based radar and airborne data were used by Willoughby and Black (1996) to illustrate mesoscale features of the South Florida landfall of Andrew, the most costly hurricane in U.S. history. Upon landfall a series of short-lived but intense convective cells formed at the northern (right) side of Andrew's inner eyewall. These cells were triggered by strong frictional convergence along the coast, and they then rotated counterclockwise around the eyewall. McCaul and Weisman (1996) explain how the near-hurricane environment may be suitable for shallow but possibly tornadic supercell storms. Powell and Houston (1998) primarily used automated surface observations and flight-level data from Air Force reconnaissance aircraft, plus a boundary layer model, to describe changes in surface wind for several landfalling hurricanes. Dodge et al. (1999b) combined nonsynchronous forward and aft beams of the vertically scanning tail Doppler radar on HRD's WP-3D aircraft to derive the wind field of Hurricane Danny as it made landfall on the Gulf Coast. They also included NEXRAD radial velocities in their synthesis, in part because the pseudo-dual Doppler airborne horizontal wind retrieval is only possible down to about 1 km above

ground level. Changes in boundary layer winds are essential to understand changes in hurricane intensity and rainfall during landfall, in particular in Hispaniola with its complex terrain. Wang and Tseng (1999) describe the radar-derived kinematic and retrieved thermodynamic field changes of Typhoon Herb (1996) as it makes landfall in Taiwan, but their dual-Doppler domain is small compared to the hurricane circulation.

A few numerical simulation experiments of landfalling tropical cyclones have been conducted by means of cloud-resolving models (e.g., Li et al. 1997). The profound scale interaction ranging from the convective to the synoptic scale, and the dynamical importance of parameterized processes (especially boundary layer fluxes and latent heating) make such simulations highly challenging. Also model validation is hampered by a lack of detailed observations. Some landfalling events near the mountainous island of Taiwan have been simulated as well (e.g., Bender et al. 1987; Lee and Jian 1999). Most of the modeling work has focused on track and intensity simulation, not on the precipitation morphology.

Certainly the landfalling process cannot be isolated from offshore hurricane dynamics. For instance, Hurricane Andrew, landfalling near Miami, happened to be in a rapid intensification phase after the inner eyewall had been replaced by an outer, fully concentric eyewall (Willoughby and Black 1996). Offshore deep convective bursts in the eyewall may be precursors to tropical cyclone genesis or intensification (Riehl and Malkus 1961; Simpson et al. 1998; Halverson et al. 1999); however, similar extreme convective events also occur during landfall (Stewart et al. 1997). Such events are not surprising in view of increased low-level convergence, and possible orographic forcing. It is not clear how this deep convection affects the evolution of a landfalling hurricane.

One unusual landfalling event is that of Hurricane Danny, which only barely reached hurricane intensity. During landfall on the Gulf Coast on 18 July 1997, Danny exhibited deep convective activity, spawned one tornado, and sustained extremely high rainfall rates. Hurricane Danny was unusual in its compact size, its intensification during landfall, as well as its flow field and low-level baroclinic structure (Kong and Elsner 1999). The Dauphin Island Sea Lab reported 660 mm of rain in 7 h, with higher amounts estimated by radar over Mobile Bay, where the hurricane was nearly stationary for about 24 h as it underwent an eyewall replacement cycle (Blackwell 2000). It was unusual also that Danny maintained a clear vortex structure long after landfall. On 22–23 July 1997 Danny spawned 12 more tornadoes, along its track from central-east Alabama to the Carolinas. The mesolow also deepened by an estimated 9 hPa during this period, possibly under the influence of a weak upper-level trough approaching from the west (Riordan and Cline 1999). In contrast to landfall on the flat Gulf or Atlantic coasts of the United States, landfall on mountainous islands, such as Hispaniola, is bound to be more complex.

3. Hurricane Georges's landfall on the Dominican Republic: Surface observations

On 22 September 1998 Hurricane Georges made landfall on the island of Hispaniola. The eye moved across the center of this island, and although Georges moved steadily at about 8 m s^{-1} and the storm weakened considerably during its passage, it became one of the worst natural disasters in the history of the Dominican Republic (DR). In the wake of the storm, 438 people were confirmed dead or missing in the DR, more than 155 000 people were homeless, and the country's main industries, agriculture and tourism, suffered gravely. The direct losses were estimated at $1.2 billion U.S. dollars by the presidential office of the DR. In the densely populated southeastern lowlands region of the DR, about 55% of the annual agricultural production was lost. Most of the damage and deaths resulted from mudslides, flash floods, and inundation of river valleys, not from extreme winds or storm surge along the coast.

Hispaniola has the same surface area as 58% of the state of Alabama, so it is large compared to a typical eyewall. It is also mountainous, with several mountain chains running mainly WNW–ESE. The main chain, the Cordillera Central, rises up to about 3.1 km. Atmospheric observing capabilities in Hispaniola are quite limited and are mostly in the DR, which occupies the eastern two-thirds of the island. An S-band radar is operational near DR's capital Santo Domingo, on the south coast, but low-level observations are limited by beam blockage by the mountains.

Before passing over the DR, Georges had affected several islands in the Lesser Antilles and Puerto Rico, but it had retained much of its circulation strength. In fact, after leaving the much smaller island of Puerto Rico, it deepened an estimated 16 hPa to 962 hPa in 12 h, before making landfall on Hispaniola. There was

considerable wind damage as a result of wind gusts up to 58 m s^{-1} at Boca de Yuma on the southeast coast (location shown in Fig. 1). In the capital Santo Domingo, on the south coast, flooding occurred due to sustained onshore winds and an ocean storm surge: at 1800 UTC on 22 September, when the eye was about 40 km to the north, a sustained wind of 37 m s^{-1} was measured. But most damaging to the DR was the extreme rainfall. For instance, around 0600 UTC on 23 September a small dam on the San Juan y Maguana river, which originates on the western flanks of the Cordillera Central, was weakened enough by the overflow to collapse, sending muddy floodwaters into a downstream community of 7000 people (Mejia and Rodriguez 1999). Fortunately most people had been evacuated to higher ground for the night, avoiding additional casualties.

Forty-eight rain gauge stations across the DR measured 24-h rainfall totals on 22 September between 0.7 and 41 cm, the maximum being measured at Santo Domingo (Fig. 1). This 24-h period covers the entire storm passage in most places except on the southern peninsula and near the western border of the DR, where a significant fraction fell on 23 September.

The maximum 1-h rainfall rate of 82 mm h^{-1} was recorded at Herrera, which is near sea level just west of the capital. It is suspected that higher hourly rain rates occurred in DR's mountainous interior. The country's north was spared from heavy rains, while flooding rains affected the south coast and the Cordillera Central. The same north–south asymmetry in rainfall amounts was observed on the much smaller island of Puerto Rico, where Georges's eye passed late on 21 September. This asymmetry is not only explained by Georges's track, which was just south of Hispaniola's central axis (Fig. 2). The asymmetry is evidence that most water vapor entered Georges from the south and that the mountainous islands acted as a barrier. The heavy rain in the vicinity of Santo Domingo partly resulted from a massive MCS drawn into the circulation from the south, after George's eye had passed. The province of Barahona on the southern peninsula also received rain from this southern moisture influx in the wake of Georges's passage, and heavy rain fell from

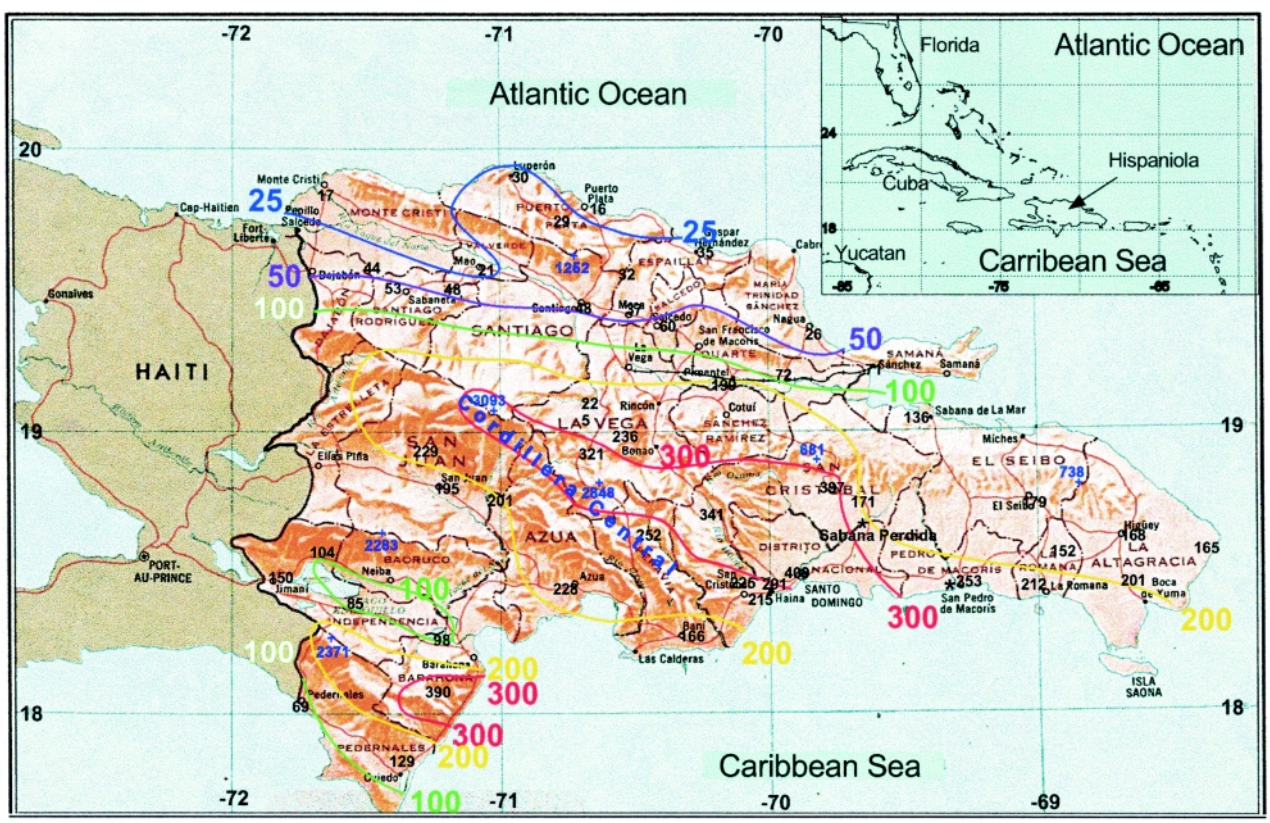

FIG. 1. Gauge-estimated rainfall totals over 24 h starting at 0000 UTC on 22 Sep 1998, and subjectively drawn isohyets at 300, 200, 100, 50 and 25 mm. The maximum height (m) of some mountain ranges is shown in blue, and the rain gauge data (in mm) are in black. The insert map in the upper right corner shows the location of the island of Hispaniola, which consists of Haiti (in the west) and the Dominican Republic.

an earlier, long-lived MCS well ahead of Georges. As a result, the wettest place over a 3-day period (21–23 September) was on the southern peninsula, in Polo, where 53 cm was recorded.

Georges's passage over the DR can truly be considered to be a landfalling case, even though Hispaniola is only an island and the hurricane recovered after crossing Hispaniola, albeit never to the same strength. Georges made landfall again on 28 September, on the Gulf Coast, at nearly the same intensity as the 22 September landfall. Radar imagery indicates that that landfall, on flat terrain, produced widespread heavy stratiform rain, with little or no deep convection. The island of Hispaniola has a cross-track width of about 250 km, much wider than the diameter of the satellite-observed eyewall (about 100 km before landfall). Especially strong interaction between air and land can be expected in this case because of the mountainous terrain.

The National Hurricane Center (NHC) issues real-time estimates of storm location and intensity. These estimates are based mainly on in situ observations by Air Force reconnaissance aircraft, satellite imagery, and the occasional station, buoy, or ship observation. The NHC may slightly alter these estimates in a follow-up preliminary report.[2] The estimated track of Hurricane Georges in the vicinity of Hispaniola is shown in Fig. 2. Other hurricanes have crossed the DR along a similar path. In 1979 Hurricane David made landfall just west of Georges's landfall on the southeastern coast of the DR, and after crossing the Cordillera Central, its minimum sea level pressure (SLP) increased from 926 to 1002 hPa. David's track departed from a straight line: a southward departure near the southeastern tip of the DR was followed by a northward deflection as the island was crossed. Bender et al. (1987) suggested that this sinuosity is related to the local topography: the island's mountains affect the basic flow as well as the storm-scale wind field, resulting in the observed deflections. Georges, starting along the same track as David, only slightly departed from a straight path as it crossed Hispaniola in the way anticipated by Bender et al. (Fig. 2).

The minimum SLP increased from 962 hPa just before landfall, at 1500 UTC, to 986 hPa just before Georges exited Hispaniola, at 0300 UTC on 23 September. It is not known how accurate or reliable the DR station data are, but some outstanding observations are mentioned. A barograph of Bayaguana (its location, adjacent to San Pedro de Macoris, is shown by a star in Fig. 1) measured a minimum SLP of 949 hPa at 1650 UTC (Mejia and Rodriguez 1999). The sky was reported to be clear and the wind calm. At 1745 UTC the eye's center passed another barograph, at Sabana Perdida (Fig. 1), where the minimum SLP was 973 hPa. Farther along Georges's track there are fewer stations. No DR station measured a SLP less than 998 hPa after 1745 UTC. Therefore the actual weakening of the hurricane circulation may be more pronounced than the real-time estimate shown in Fig. 2. And the NHC estimate of the change in maximum sustained surface wind speed, from 54 to 36 m s^{-1}, may also be an underestimate.

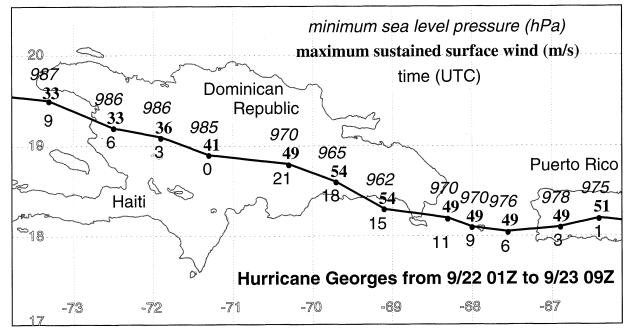

FIG. 2. Track of Hurricane Georges from 0100 UTC on 22 Sep to 0900 UTC on the next day, with estimated maximum sustained surface wind (m s^{-1}) and minimum SLP (hPa). The data are estimates by the National Hurricane Center, except for the positions at 2100 and 0000 UTC,which are slightly different from the NHC estimate. The corrections are based on EDOP velocity data.

4. Aircraft operations

During August and September 1998 the National Aeronautics and Space Administration (NASA) joined efforts with HRD in the Third Convection and Moisture Experiment (CAMEX-3). CAMEX-3's main objective was to obtain detailed in situ and remote airborne observations serving to better understand tropical cyclone development, tracking, intensification, and landfalling impacts. CAMEX-3 operations focused on two NASA aircraft. The DC-8 was equipped with a host of instruments including a cloud and aerosol particle spectrometer, a water vapor profiler (differential absorption lidar), a clear-air wind retrieval system (Doppler lidar), a microwave radiometer, dropsondes, electric field detectors, and a scan-

[2]The preliminary report on Georges is available online at http://www.nhc.noaa.gov/1998georges.html.

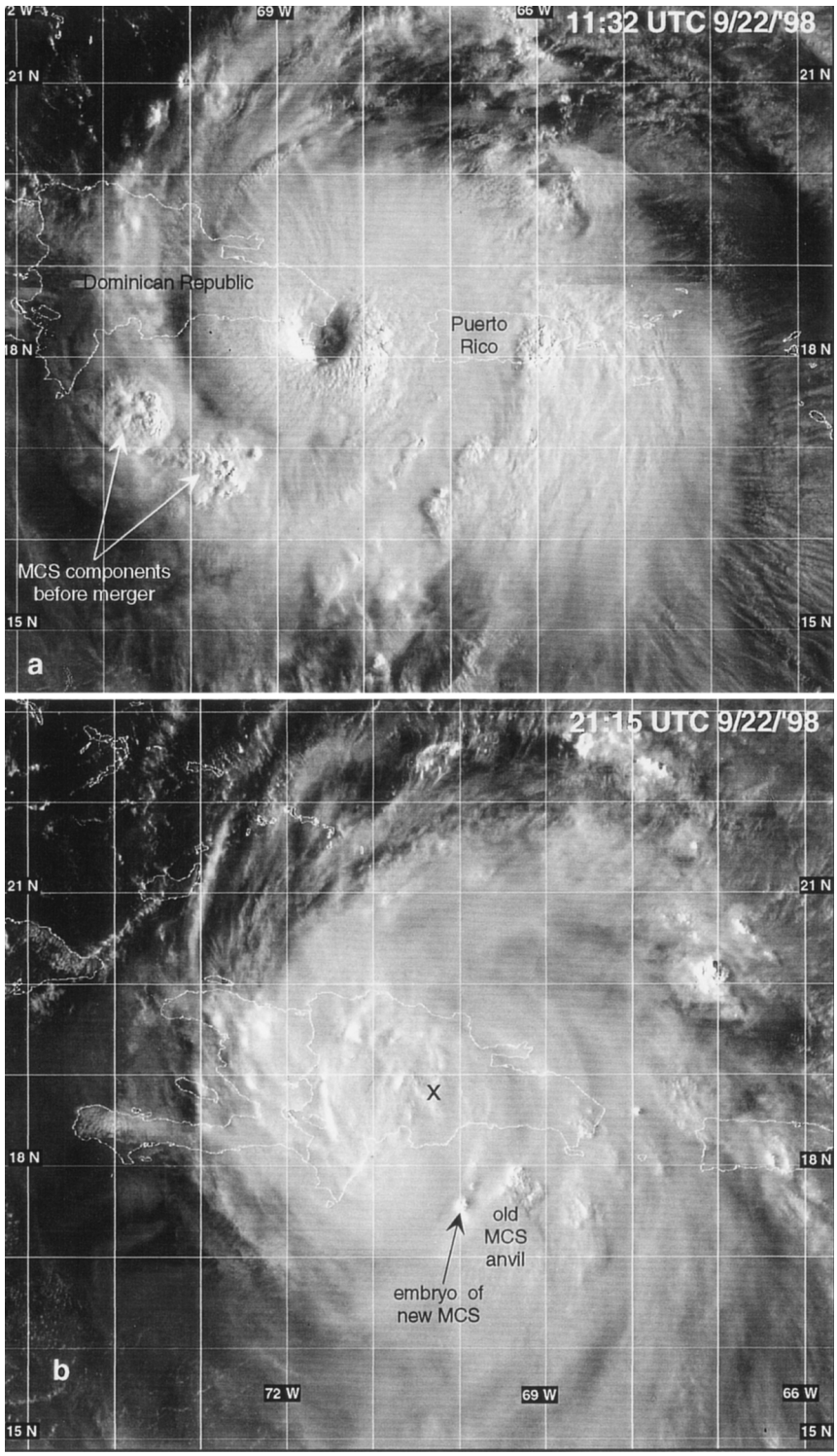

FIG. 3. *GOES-8* visible imagery at (a) 1132 and (b) 2115 UTC.

ning K_u-band Doppler radar. The ER-2, a small single-pilot jet flying at about 20 km above sea level, was equipped with visible, infrared, and microwave imagers; electric field detectors; an interferometer (to retrieve temperature and moisture profiles); and a nadir and forward looking X-band Doppler radar. Reflectivity and radial velocity estimates from the latter, the EDOP, are the focus of this study. Because the ER-2 flies steadily above all convection, the effect of aircraft motion on the measured Doppler velocities is fairly small. EDOP data are unique for their superb vertical resolution, their high sensitivity, and their clutter-free nature down to ground level.

Several reconnaissance and research aircraft visited Hurricane Georges on 22 September. Two NOAA aircraft (the Gulfstream-IV and the WP-3D N43RF) flew a synoptic surveillance pattern and together they deployed 47 dropsondes in the broad vicinity, too far to collect Doppler radar data of Georges over Hispaniola. The NASA DC-8 flew through the storms's eye at about 11 km and then examined the storm inflow to the south, east (Mona Passage), and north. Finally, the NASA ER-2 made four passes over the eye or its remnants between 2000 and 2300 UTC.

5. Large-scale evolution

a. GOES-8 *and ground radar imagery*

An eye was clearly evident in satellite imagery before landfall and even while Georges moved along the southeast coast of the DR between 1100 and 1600 UTC. A comparison of the morning and evening visible satellite images (Fig. 3) shows some dramatic changes in the cloud-top structure. At 1132 UTC a clear eye and eyewall could be seen, and radial cirrus striations suggested divergence from the eye. At 2115 UTC, both the eye and the divergent flow aloft were no longer

apparent, and the smooth cloud-top undulations near the center of the circulation indicate mature convection and/or stratiform precipitation.

The details of the eye-filling process are revealed by *GOES-8* satellite IR (4 km) and visible (1 km) bihourly imagery, as well as by hourly survey scans from a noncoherent S-band radar in Santo Domingo. The three graphs in Fig. 4 analyze the changes in satellite IR cloud-top temperature. Pixels within 22, 100, and 300 km from the best-guess center of circulation were classified according to their brightness temperature (T_b). The radii are somewhat arbitrary and represent the eye, the eyewall, and the entire cyclone, respectively. Satellite IR imagery, as well as the EDOP and passive microwave data, suggest that the diameter of the eye does not change much. Even so, the eye becomes increasingly ill-defined after landfall, so the "eye" in Fig. 4c merely refers to an area within 22 km from the best-guess center of circulation. The eight graphs in Fig. 5 show changes in the eye and eyewall as seen by the Santo Domingo radar. These graphs suggest that most rain falls offshore, at all times. While offshore intensification of eyewall and spiral bands is plausible, caution must be exercised in the interpretation of Fig. 5, because of significant ground clutter and beam blockage. Also, the radar resolution (2.1° beamwidth) and sensitivity (~3 dB) are rather poor. Nevertheless the data are useful because of the unique radar location with regard to landfall.

The warming of the eyewall cloud top between 1200 and 1600 UTC (Fig. 4b) suggests a weakening, yet the minimum SLP decreased by ~7 hPa during this period. Between 1600 and 2300 UTC, while the hurricane moved over land and the mountains, the overall cloud-top signature within 100 km of the center changed little. The eye passed the crest of the Cordillera Central around 2200 UTC, and after 2300 UTC the cloud top started to warm. This trend continued until 0800 UTC on 23 September (not shown in Fig. 4b). At this time about half of the area within 100 km of the center had $-55°C < T_b < -35°C$, compared to only 16% of the area at 2345 UTC. This warming implies subsidence and/or thinning of the cloud top. These are signs of weakening convection.

Within the eye (Fig. 4c), some clouds appeared in the visible and IR images at 1345 UTC, with T_b as low as −45°C. These clouds are nonprecipitating according to the radar imagery and decayed by 1445 UTC. New clouds appeared within the eye at 1515 UTC. These clouds grew colder (i.e., higher) between 1545 and 1745 UTC, as seen in the trend of the $-55°C < T_b$

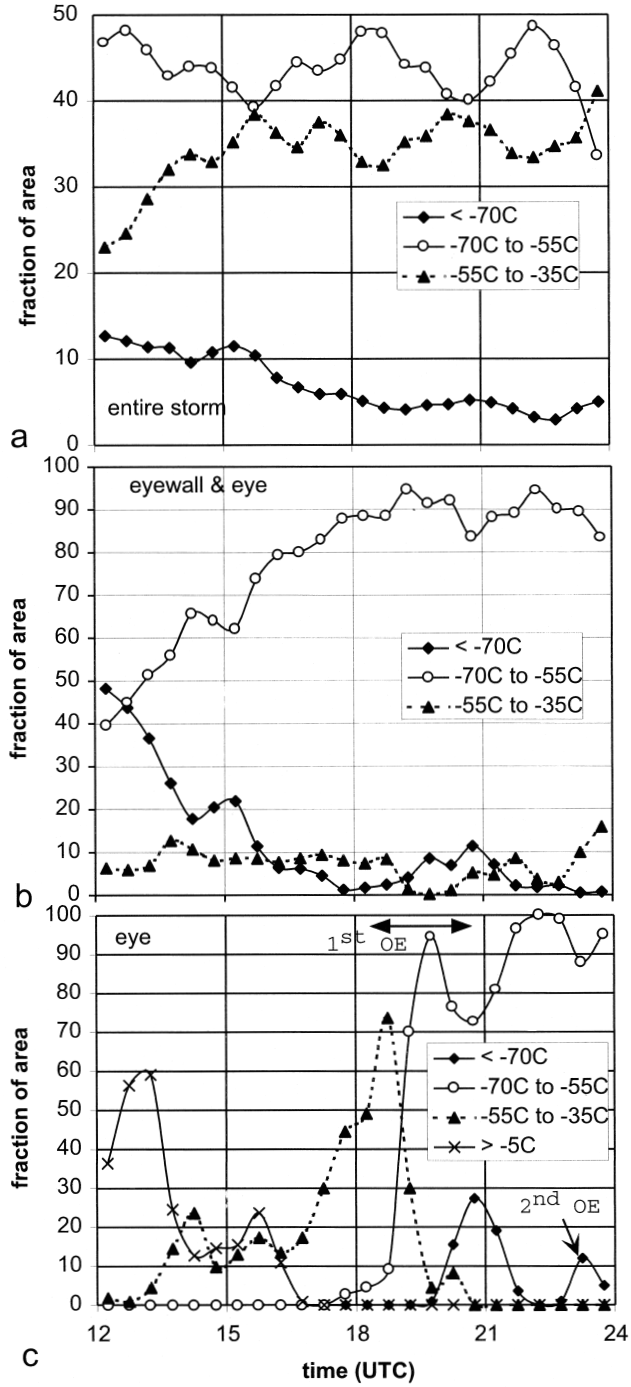

FIG. 4. Analysis of *GOES-8* IR imagery for a 12-h period starting at 1200 UTC on 22 Sep. The fraction of the areas with IR brightness temperature less than −70°C, between −70°C and −55°C, and between −55°C and −35°C is shown for (a) the entire storm (within a 300-km radius from the center of Georges's primary circulation), (b) the inner storm (within a 100-km radius), and (c) the eye (within a 22-km radius). Also shown in (c) are the fractional area with $T_b > -5°C$, and two events of overshooting convection in the eye (OE).

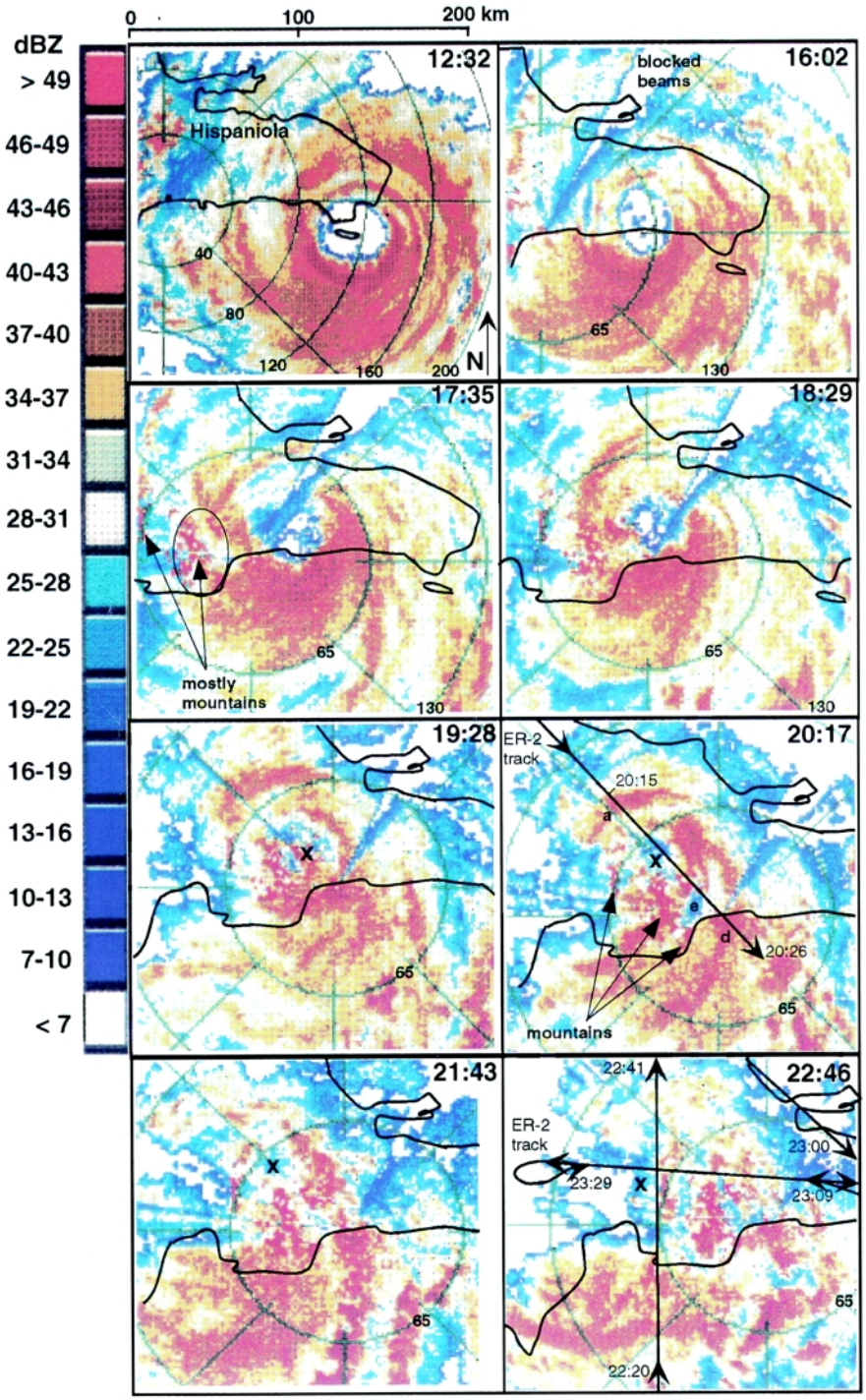

FIG. 5. Reflectivity images from the Santo Domingo radar scanning at 0.5° elevation. The times of observation are shown in UTC in the upper-right corner of each image. The black line is the Hispaniola coastline. The "x" in the last four images indicates the location of the eye. The ER-2 track is superimposed on the 2017 and 2246 UTC images. The letters on the 2017 UTC image refer to features described in the text.

< −35°C bin in Fig. 4, yet they remained well separated from the eyewall. This suggests that they were generated convectively within the eye. Not much rain appeared to fall from these clouds, according to the 1602 UTC radar image (Fig. 5). Eventually this convection (or at least its tops) spun outward and merged with the eyewall by 1745 UTC, at which time the lowest IR T_b of this convection was −71°C, that is, near tropopause level. At 1735 UTC light rain from this convection occurred over much of the eastern half of the eye (Fig. 5).

The first intrusion of clouds in the eye (around 1400 UTC) reduced the cloud area with $T_b > -5$°C (which represents the cloud-free fraction) from about 60% to less than 20% of the eye (Fig. 4c). The second event (around 1600 UTC) caused the area with $T_b > -5$°C to vanish within the eye. By 1745 UTC, satellite imagery shows the eye entirely filled, and half of the eye's area (i.e., a circle with a 22-km radius) measured cloud tops colder than −35°C. The local weather report in the eye at this time, at Sabana Perdida (Fig. 1), mentions six octas of cloudiness, no rain, and no wind (Mejia and Rodriguez 1999).

Around 1900 UTC the center of the circulation reached the eastern margin of the Cordillera Central. High clouds rapidly covered the eye, within 30 minutes (Fig 4c). The question is whether these cold cloud tops advected from the eyewall or were the result of local deep convection. At 1928 UTC, heavy rain fell in a small area near the eye's center (Fig. 5). Further evidence of the local convective nature of these clouds comes from EDOP data across the eye around 2015 UC (see below). EDOP data and the 2045 UTC IR image indicate that some of the eye convection towered above the eyewall anvil level. Very cold cloud tops (colder than −70°C) occupied about 25% of the eye's area at this time

(Fig. 4c). This burst of convective activity is labeled as the first overshooting event (OE) in Fig. 4c. The EDOP data suggest a second burst in or near the eye around 2315 UTC, when the eye is above the Cordillera Central. This burst is rather weak in the eye statistics (Fig. 4c), and cannot be seen in the Santo Domingo radar data on account of beam blockage to the northwest of the radar. However, ER-2 instruments collected a marvelous record of this surprisingly strong event.

b. Satellite microwave data

Microwave radiation at 85.5-GHz upwelling from cloud tops provides information on the ice path, which depends on the concentration, habit, and size of ice particles in a column of cloud (Spencer et al. 1989). In deep convective clouds with strong ice scattering, the 85.5-GHz brightness temperature can be more than 100 K below the actual cloud top temperature. Low brightness temperatures have been shown to relate well to high radar reflectivities above the bright band (e.g., Heymsfield and Fulton 1988; Mohr et al. 1996). Because Hurricane Georges is partly over water and partly over land, and because surface water has a lower emissivity at 85.5 GHz than land, it is necessary to distinguish between low brightness temperatures caused by background effects, rather than by ice scattering. However, microwave scattering by ice particles is so intense in the deep clouds associated with Hurricane Georges that this difference can be ignored (Heymsfield et al. 1996b).

Spaceborne microwave data were available from both the SSM/I (Special Sensor Microwave/Imager) and the TMI (TRMM Microwave Imager) instruments on different satellites (Table 1). Between 0310 and 1033 UTC on 22 September, before landfall, the 85.5 GHz T_b slightly increased in the eyewall (111-km radius) and in the entire storm region (333-km radius). After landfall, at 0125 UTC on 23 September, the average T_b was significantly higher, but the minimum T_b was much lower; in other words, vigorous convection had developed in an otherwise declining hurricane. During the period spanning the landfall on the DR (from the second to the third entry in Table 1), the average rain rates in the eyewall region and for the entire storm (a 333-km radius around the eye) decreased by a factor of 3 and 4, respectively. These rain rates were estimated using the Goddard profiling algorithm, which is based on upwelling microwave radiation at 85.5 GHz and other frequencies (Kummerow and Giglio 1994). Yet at 0125 UTC on 23 September relatively cold brightness temperatures were measured over or near the Cordillera Central by the F14 SSM/I probe: four pixels (13 × 15 km each) had a $T_b < 160$ K.

Further weakening occurred when Georges moved over Haiti: at 1358 UTC on 23 September, the eyewall diameter had become very large (~180 km), and little rain fell within 111 km from the center (2.7 mm h^{-1} on average). Ice scattering and rain rates associated with Georges increased as the hurricane moved over the Windward Passage, even in remote rainbands, but then weakened again after landfall on Cuba. At 1816 UTC on 23 September, the northeastern quadrant of Georges had no eyewall, and estimated rainrates did not exceed 30 mm h^{-1} anywhere, except for a small area of intense convection over the Sierra Maestra in southeastern Cuba.

TABLE 1. Average and minimum 85.5-GHz brightness temperatures (K) as measured by the Special Sensor Microwave/Imager (SSM/I) probe on the Defense Meteorological Satellite Program (DMSP) satellites F13 or F14, or by the TRMM Microwave Imager (TMI) instrument aboard the TRMM (Tropical Rainfall Measuring Mission) satellite. The domains of interest, labeled "eyewall" and "entire storm," are in a circle with a radius of 111 and 333 km, respectively, centered on Hurricane Georges. The fraction of the entire storm covered by the observation swath is listed in the last column. TMI and SSM/I 85.5-GHz radiance data are equivalent, the only difference is the higher resolution of the TMI data. Georges made landfall around 1600 UTC on 22 Sep.

Time and date (UTC)	Location of Georges's eye	Instrument	Mean 85.5-GHZ T_b		Minimum 85.5-GHz T_b		% coverage
			Eyewall	Entire storm	Eyewall	Entire storm	Entire storm
0310 22 Sep	Puerto Rico	TMI	230.8	250.0	169.3	114.8	71
1033 22 Sep	Mona Passage	SSM/I (F13)	234.6	255.3	184.9	136.1	100
0125 23 Sep	DR	SSM/I (F14)	245.5	267.5	142.7	142.7	97
1358 23 Sep	Bay of Haiti	SSM/I (F14)	266.3	263.3	226.9	148.8	100
1816 23 Sep	Windward Passage	TMI	248.3	255.8	140.2	140.2	100
2258 24 Sep	Cuba	SSM/I (F13)	256.0	262.2	219.7	210.3	100

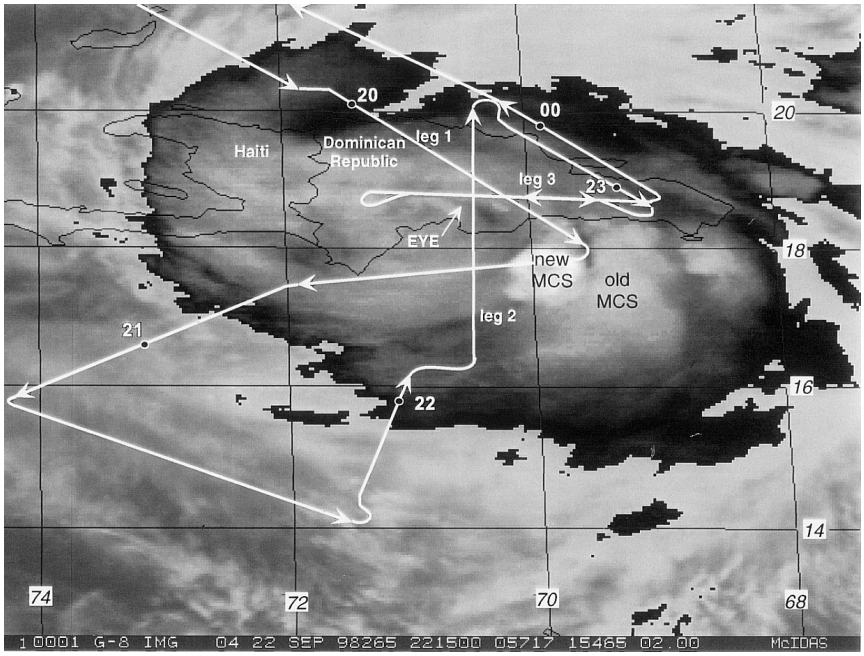

FIG. 6. Track of the NASA ER-2 superimposed on a *GOES-8* IR image at 2215 UTC. The arrows indicate the direction of flight. White numbers adjacent to the track are hours (UTC), and ER-2 flight legs 1–3 are labelled. The location of the eye at 2215 UTC is estimated based on airborne and ground-based radar imagery. The IR image is enhanced to highlight the coldest cloud tops: the enhancement ranges from −42°C (black) to −83°C (white).

Satellite microwave imagery suggests that much rainfall occurred to the south of the DR during the passage of Georges over the island, on account of several episodes of mesoscale convective activity. A large, long-lived, almost circular mesoscale convective system (MCS) dominated the scene. This MCS resulted from two separate clusters of overshooting towers growing just south of the DR between 0800 and 1000 UTC, about 250 km ahead of Georges's eye. These two clusters, which can be seen at 1132 UTC between 16°–18°N and 69°–71°W (Fig. 3a), merged into a single cloud anvil around 1200 UTC. The MCS had cloud-top temperatures well below that of the eyewall; in fact it is responsible for most of the area with IR $T_b < -70$°C in Fig. 4a. It reached its maximum size of about 38 000 km^2 ($T_b < -52$°C) at 1500–1600 UTC, and slowly wrapped around and closed in on Georges during the next 8 h. It shrunk and weakened somewhat during 1500–1900 UTC, but a cluster of renewed activity, slightly closer to the eye than the old center of activity, kept it active until 0200 UTC on 23 September, when it decayed over the south coast of the DR near Santo Domingo. The embryonic stage of the new cluster is highlighted by the setting sun in Fig. 3b near 17.6°N, 70°W. This cluster was slightly smaller than the original MCS, but the Santo Domingo radar indicates heavy rainfall from a weakly organized system. This cluster (shown as "new MCS" in Fig. 6) climaxed around 2300 UTC, after which it merged with the older MCS. At 2302 UTC, about 40 min after sunset, the ER-2 pilot reported seeing spectacular purple lightning flashes, emanating above cloud top (but below flight level), from a location that appears to be the northern part of the MCS (where the T_b was lowest), just off the coast of the DR.

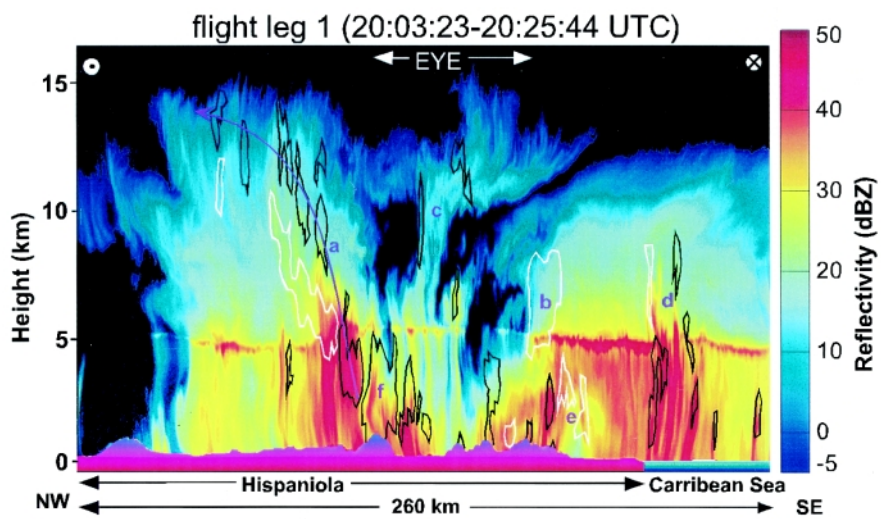

FIG. 7. EDOP nadir reflectivity cross section for the first ER-2 pass over the DR (leg 1 in Fig. 6), from northwest to southeast, around 2015 UTC. Solid black (white) contours delineate areas with updrafts (downdrafts) of 4 m s^{-1} or more. The rugged topography of Hispaniola is apparent. Several mountain ranges (up to ~1 km high in this section) are overflown. The letters a–f refer to features described in the text. The direction of the primary hurricane circulation is shown in the upper corners. The horizontal scale much exceeds the vertical scale.

6. EDOP observations

EDOP has a wavelength of 3.12 cm (9.6 GHz), a vertical resolution of 37.5 m, and a horizontal along-track resolution of about 550 m at 10 km MSL and 1100 m at the ground. However, the sampling rate converts to a beam spacing of just 100 m (Heymsfield et al. 1996a). EDOP has two fixed antennas: nadir and forward (34° from nadir). The accuracy of EDOP reflectivity values has been confirmed by comparison with other radars (Heymsfield et al. 2000). The 2D (along track) airflow field can be synthesized from the radial velocities of both beams. The forward antenna receives both the vertically and horizontally polarized return. It is primarily the high vertical resolution that distinguishes EDOP from other radars.

EDOP data from three flight legs over Georges are shown in Figs. 7–10. EDOP reflectivity data are not corrected for attenuation, which is negligible for beam reflectivities below 45 dBZ. Also shown in Figs. 8 and 10 is the Doppler velocity from the nadir antenna, corrected for aircraft motions. For instance, an upward pitch of the aircraft would introduce a fraction of the aircraft's forward movement as a negative component (toward the radar) in the radial velocity of the nadir antenna (Heymsfield et al. 1996a). After adjustment for aircraft motions, the vertical motion field is fairly accurate, except in the case of large ER-2 angle excursions, which did not occur on the flight legs over Georges. After this correction the nadir Doppler velocity merely represents vertical hydrometeor velocity, which includes both the terminal velocity (fall speed) of the hydrometeors and vertical air motion. The hydrometeor fall speed can be estimated from relations between reflectivity and fallspeed, but there is considerable uncertainty related to drop size distribution and ice density. For the first EDOP passage over Georges (Fig. 7), the fall speeds were estimated by means of the relationships by Black et al. (1996, p. 1890) for hurricanes and then removed to reveal the vertical air motion.

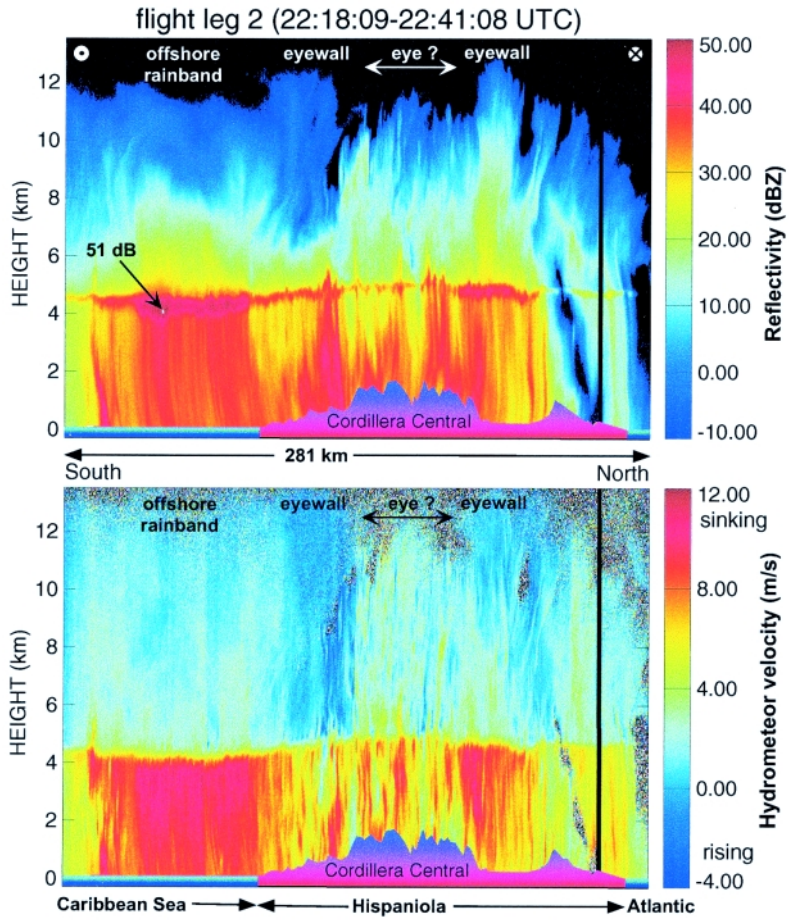

FIG. 8. EDOP nadir reflectivity (upper panel) and nadir Doppler velocity (lower panel) in a south–north section across the Caribbean Sea and the DR and its main mountain ridge (leg 2 in Fig. 6) around 2230 UTC. A contoured frequency by altitude diagram (CFAD) for the width shown by the thick purple horizontal line below the reflectivity section is given in Fig. 9a.

The ER-2 also carried two scanning microwave imagers on this flight, the Advanced Microwave Precipitation Radiometer and the Millimeter-wave Imaging Radiometer (MIR). Data from the latter only are available for all legs across Georges's eye and are shown in Fig. 11. The frequency of the MIR ice scattering channel is slightly higher (89 GHz) than that of TMI (85.5 GHz), but the behavior of ice scattering is nearly identical at both frequencies.

a. Leg 1

The ER-2 first flew over Georges around 2015 UTC (leg 1 in Fig. 6), when the "eye" was covered with cold clouds (Fig. 4) and had become difficult to locate even on radar imagery (Fig. 5). The horizontal wind field derived from the EDOP forward beam confirms that this pass came very close to the center of the hurricane circulation: the average storm-relative wind speed in this section is near zero. The eye region shown in Fig. 7 is inferred from both reflectivity and

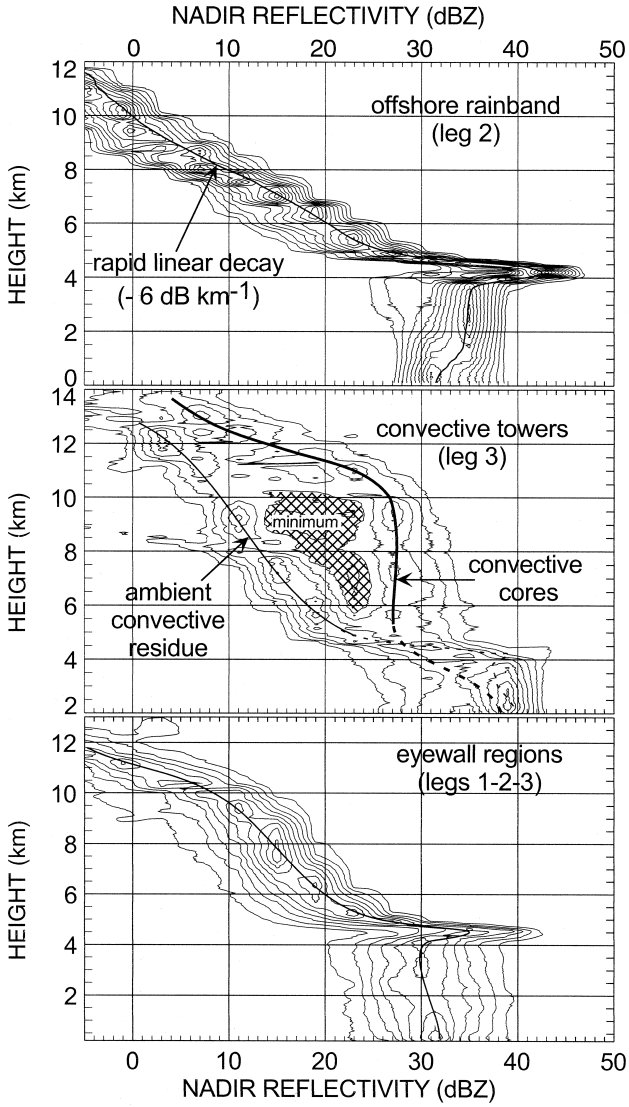

FIG. 9. Reflectivity CFAD for (top) the band of heavy stratiform rain offshore (leg 2), (middle) the convective towers within the eye over the Cordillera Central (leg 3), and (bottom) a composite of eyewalls and surrounding onshore stratiform regions in legs 1–3. The region over which a CFAD is calculated is shown by a purple line in Figs. 8 and 10 for (top) and (middle), respectively. The composite (bottom) consists of the southeastern eyewall of leg 1, the northern eyewall of leg 2, and the eastern eyewall of leg 3, and has a total length of 158 km. For all CFADs the reflectivity bin size is 4 dBZ and the contour interval 40. The solid thick line in (top) and (bottom) is the mean reflectivity. The thick lines in (middle) interpret the bimodal distribution of reflectivity above the freezing level.

velocity fields. It is marked by a low-level confluence of opposing winds, first from the northwest and then from the southeast.

About one hour before this pass the eye had suddenly been covered by cold cloud tops (Fig. 4c). At the time of the pass, the minimum *GOES-8* IR T_b was –75°C, which is the tropopause temperature in the 1200 UTC sounding at Santo Domingo on 22 September. The eye was still on the eastern side of the Cordillera Central. EDOP reveals an eye that is highly disturbed at low levels, with several narrow rainshafts reaching up not much higher than the freezing level (Fig. 7). These rainshafts show a clear bright band, suggesting that they are not associated with strong updrafts. A large anvil with echo tops above 15 km covers most of the eye. This anvil appears to have arisen from convection *within* the eye, and the anvil shape and bright band suggest that this convection has decayed. The base of this convection may have eroded at the time of the overpass. The upper parts of the anvil appear to be spreading to the southeast in the upper-tropospheric divergent outflow, and much of the anvil is subsident, except for two upper-level updraft cores (near "c" in Fig. 7).

The eyewall had become highly asymmetric in this first cross section. It was convective at the northwestern end, with a broad, slanting updraft ("a" in Fig. 7), yet it was more shallow and stratiform at the southeastern end, where the air subsided at mid levels ("b" in Fig. 7). This asymmetry is apparent in the MIR imagery as well (Fig. 11), with stronger ice scattering (160 K < T_b < 200 K) on the northwest side. The topography may explain the asymmetry. The Cordillera Central is approximately parallel to this section, and just upstream on the NW side but downstream on the SE side. This topography also explains a small, nearly rain-free region in the southeastern eyewall (labeled "e" in Fig. 7). This rain "shadow" is part of a larger clearing east (downstream) of the main cluster of mountain peaks visible in Fig. 5. This rain shadow is capped by subsiding air, resulting in cloud-free conditions and raindrop evaporation. The shadow and the downdrafts in Fig. 7 do not quite coincide; this may be due to large horizontal (into the page) advection. Updraft core "F" in Fig. 7, located just within the eyewall, coincides with the main mountain in the cross section. The updraft strength (peaking at 8–10 m s^{-1}) and associated reflectivity suggest that this is a young feature. All updrafts in Fig. 7 are rather large in diameter in comparison to a large sample of drafts in intense hurricanes summarized in Jorgensen et al. (1985).

Oscillations in the height of the bright band represent local temperature anomalies. Within the eye the bright band was about 0.5 km higher than elsewhere. This implies a temperature anomaly of about +3 K (assuming a moist adiabatic lapse rate of 6 K km^{-1}). The

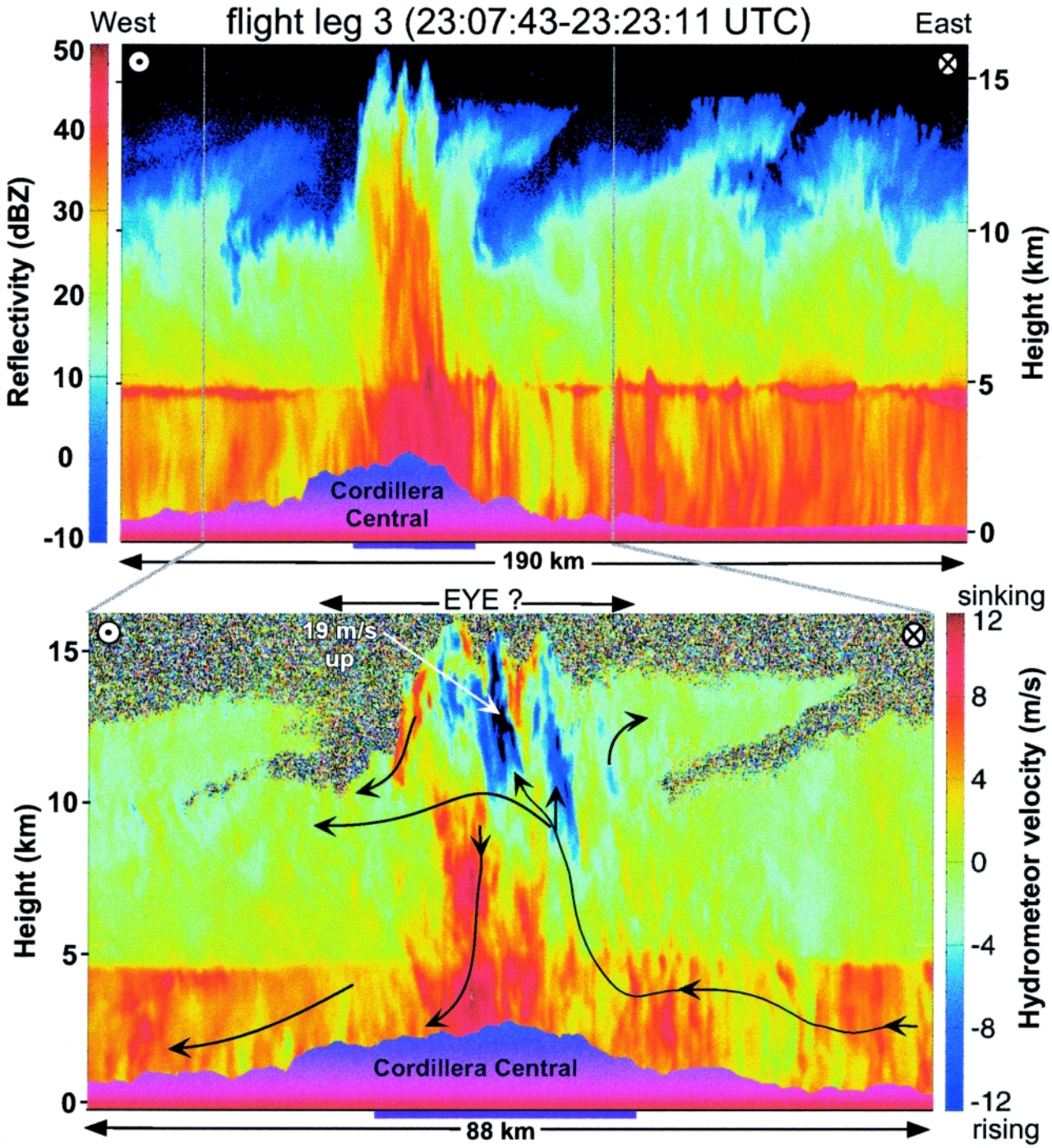

FIG. 10. As Fig. 8, but for an east–west section (leg 3 in Fig. 6) and about 45 min later. The black lines with arrows are streamlines, estimated from EDOP's nadir and forward radial velocities.

NASA DC-8 flying simultaneously along the same track at 11 km measured an anomaly of about +2 K relative to the eyewall. These figures are small compared to the 6-8 K anomaly found on three flight legs at the same level across Hurricane Georges just before it reached Puerto Rico on 21 September. This weakening of the upper-tropospheric warm core is consistent with the observed decline of the hurricane's intensity after landfall.

The heavy rain and supporting updrafts (d in Fig. 7) offshore, just south of Santo Domingo, are also apparent in radar and satellite imagery. The echo tops south of Hispaniola were about 13 km (about −54°C), which corresponds well with the satellite IR cloud top there.

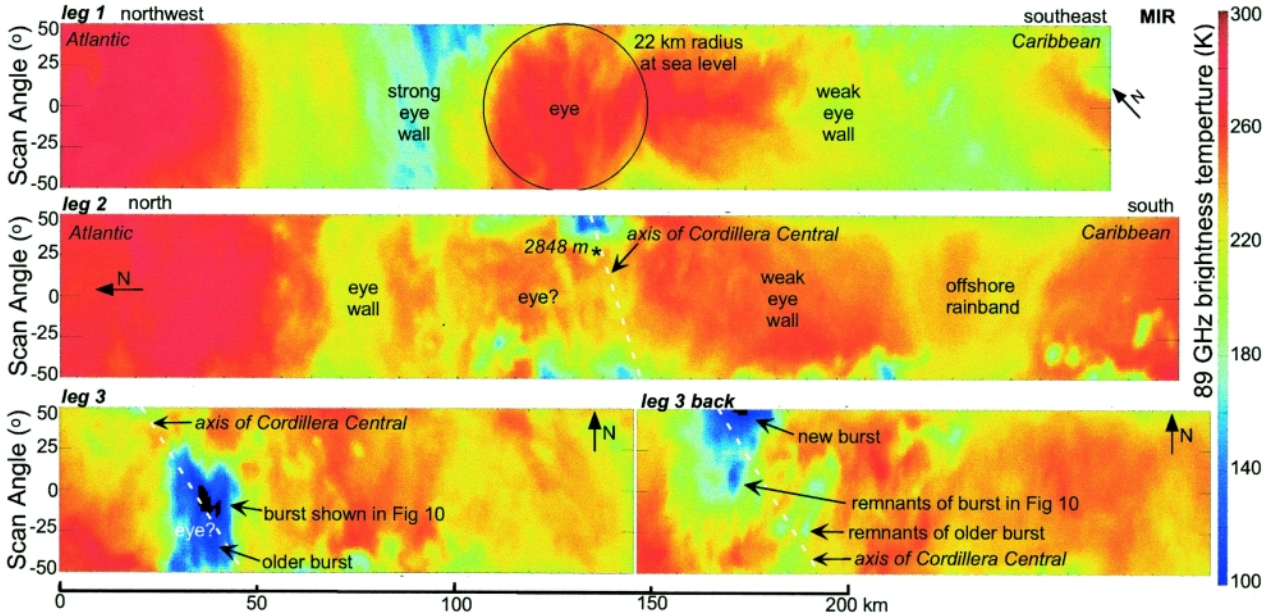

FIG. 11. 89-GHz brightness temperature derived from a scanning Millimeter-wave Imager Radiometer (MIR) on the ER-2, for the three legs shown in Figs. 7, 8, and 10, and the last leg in reverse (see Fig. 6). The length of each leg is mapped to a common scale, and legs' orientation is shown. The images represent map views, but they are compressed in their length direction. The cross direction (vertical on the page) is linear in scanning angle, and its total distance is about 40 km at sea level and 20 km for cloud tops at an altitude of 10 km. Text in italics refers to topographic features. The time and duration of legs 1 and 2 are the same as those mentioned in Figs. 7 and 8. Leg 3 is slightly shorter than the reflectivity image in Fig. 10, such that the geographic domains of "leg 3" (2310–2321 UTC) and "leg 3 back" (2326–2345 UTC) are exactly the same.

Ground-based radar images indicate that heavy rain continued to fall offshore south and west of Santo Domingo during the following 3 h. This system gradually organized itself into a rainband (Fig. 5), which then moved to the southeast (away from the eye) after 2300 UTC, trailed by weaker stratiform rain, and preceded by a more vigorous cluster of cells, corresponding with the "new MCS" in Fig. 6.

b. Leg 2

The ER-2 flew northbound over this offshore rainband around 2230 UTC (leg 2 in Fig. 6). Notwithstanding its high reflectivity, this band was entirely stratiform, with a uniform reflectivity around 36 dB in the rain region, a well-defined bright band, and a uniform, rapid decay of reflectivity above the bright band (Fig. 8). A contoured frequency by altitude diagram (CFAD; Yuter and Houze 1995) of the reflectivity in this rainband shows a narrow reflectivity spectrum, a rapid linear decay above the bright band (about –6 dB km^{-1}), and a well-defined, strong bright band (Fig. 9a). Attenuation correction would add up to 1 dB to the mean profile below the bright band, and up to 2 dB to the lowest gates of the beams with the highest reflectivity values. The stratiform reflectivity CFAD and the uniformly slow settling of hydrometeors indicate that above the bright band the echo is snow. The rapid decay of reflectivity above the bright band indicates active growth and aggregation of snowflakes as they descend toward the freezing level (Stewart et al. 1984). The high brightband reflectivity, as much as 51 dBZ, is a signature of large melting snowflakes that have a large radar cross section (Willis and Heymsfield 1989). The uniformity in reflectivity at all levels is consistent with a broad, stratiform ascent. Indeed, the hydrometeor vertical motion field too appears very uniform at all levels. The average (mesoscale) observed snow motion in the rainband is downward at all levels, and the derived vertical air motion is negligibly small near the freezing level (5 km), rising to about 1.1 m s^{-1} (upward) at 9 km. Houze (1993, p. 197) defines stratiform precipitation as resulting from updrafts less than the fall speed of ice and snow. By this definition, this rainband is definitively stratiform, notwithstanding the heavy rainfall at the ground. The inferred mesoscale updraft is strong, but not exceptionally strong, in comparison with other stratiform regions in hurricanes, for which Black et al. (1996) found an average updraft of 0.2–0.3 m s^{-1} with a standard deviation of 1–2 m s^{-1}.

In short, snow crystals in this rainband settled very slowly, as they were partly suspended by the mesoscale updraft, which also sustained their continuous growth. This explains the large vertical reflectivity gradient. Just above the freezing level the snowflakes aggregated, producing large raindrops.

At the time of the ER-2 overpass shown in Fig. 8, the eye was over the Cordillera Central, and the high anvil that covered the eye between 2000 and 2200 UTC (Figs. 3c and 7) had largely vanished. Hurricane features are nearly impossible to identify in both EDOP and MIR (Fig. 11) data. In the two hours between legs 1 and 2, the 89-GHz T_b over the eyewall had increased considerably, yet the EDOP-estimated reflectivity near the ground under the eyewall remained about the same (36 dB*Z* on average in both legs). Some deep convective cells can be seen off-nadir in Fig. 11, especially in the vicinity of the eye, over mountainous terrain. There were also some cells south of the offshore rainband.

The eyewalls are more apparent in the Doppler velocity field (bottom panel of Fig. 8) than in the reflectivity (top panel): above the bright band air rises at about 1.3 m s^{-1} in the southern eyewall and 0.6 m s^{-1} in the northern one. These are averages over 20-km widths based on the fall speed relationship in Black et al. (1996, p. 1890). The vertical motion field is more disturbed than in the offshore rainband (Fig. 8, lower panel). Several low-level updrafts can be seen as light green (or blue) columns. These appear to be orographically triggered. Evidence for this is their location, generally near mountain peaks, and on radially upslope sides on both sides of the eye. There are one or two low-level downdrafts as well, but on average the air below the freezing level is clearly rising over the entire Cordillera Central. Rain streaks curve toward the north in the offshore rainband, especially close to the ground, suggesting strong low-level radial inflow. EDOP forward beam data reveal a low-level southerly jet, peaking at ~25 m s^{-1} at an altitude very close to the sea surface, below the rainband. This jet accelerates slightly toward the coast but decelerates rapidly onshore. In Santo Domingo, along the coast just to the east of this section, the southerly component of the hourly observed wind between 1800 and 2200 UTC ranged from 17 to 34 m s^{-1}. To the north of the eye rainstreaks are curved in the opposite direction, but not as much, that is, the low-level flow is convergent in the eye.

Notwithstanding the clear low-level convergence, convective cells rose only to about 11 km at this time over the mountains. These cells appear to penetrate into layers that had subsided within the eye. The net (mesoscale) vertical motion above the bright band over the mountains is very small, possibly downward.

c. Leg 3

When the ER-2 crossed the same mountains about 45 min later from the east (leg 3 in Fig. 6), a massive convective cell had mushroomed over the Cordillera Central, with a reflectivity of 35 dB*Z* as high as 12.6 km (Fig. 10). The MIR registers a very cold 89 GHz T_b (< 100 K) over this cell (Fig. 11), suggesting large concentrations of ice aloft. Ice was lofted at velocities up to 19 m s^{-1} by an even stronger updraft. Updrafts were surrounded by compensating downdrafts, indicating that the rising bubbles were buoyancy driven. Orographic forcing again was evident in the estimated low-level flow shown as streamlines in the lower part of Fig. 10. This cross section is slightly to the north of the center of the circulation at this time, so the flow has an easterly component almost everywhere. The strongest easterlies (~30 m s^{-1}) occur above the freezing level just west of the massive convective cell. There is little wind shear in this section, as evidenced also by the vertical fall streaks. Rising (descending) low-level motion can be seen over the mountain ridge as the terrain rises (sinks). The heavy rain too is slightly offset to the east of the Cordillera.

On top of the massive convective cell are three towers, one of which reaches 16.2 km (0 dB*Z* echo top), 2–3 km higher than the surrounding anvils. The tropopause in the 1200 UTC sounding at Santo Domingo on 22 September is at about 16 km. The reflectivity CFAD for a 30-km long section centered on this massive cell is shown in Fig. 9b. This CFAD is very different from the one for the offshore rainband. There is no bright band. The reflectivity is higher, on average, above the freezing level, and its distribution is broader. This distribution is distinctly bimodal: the higher maximum corresponds to the convective core, where strong updrafts carry hydrometeors to high levels, possibly producing graupel. The CFAD offers a hint that graupel (or other ice of higher density than snow) may be present: the reflectivity increases by ~6 dB downward across the freezing level. Graupel does not melt immediately and does not change much in size, but a wet coating would increase the reflectivity by 6.7 dB due to the difference in index of refraction between ice and water.

Equally important in the CFAD of the massive convective cell is what is called "convective residue"

in Fig. 9b. It has a much lower reflectivity and may consist of entrained stratiform precipitation or remnants of a previous convective event. The reflectivity profile of this convective residue is more stratiform in appearance: the distribution is narrow and the profile shows a linear decay with height, albeit at a lower rate than in the offshore rainband (about 2.5 dB km^{-1}). In fact the median reflectivity profile of this convective residue, highlighted by the thin solid and dashed lines in Fig. 9b, perfectly matches that of the stratiform eyewall region to the east (right) of the Cordillera Central in Fig. 10. The main differences between this profile and that of the offshore rainband (Fig. 9a) are that the reflectivity decays more slowly with height above the bright band, and that the reflectivity continues to increase below the bright band, down to the ground.

The ER-2 repeated this leg in the opposite direction (Fig. 6) and about 13 min later flew over the same massive convective cell over the Cordillera (not shown). At this time upper-level updrafts had given way to mainly downdrafts, the 35-dB*Z* contour had fallen back to ~8 km, and the 0-dB*Z* echo top was at about 15 km and was more level. There were some mid- and low-level updrafts, but downdrafts were widespread and the center of hydrometeor mass had subsided. Large and abrupt changes in the electric field (~0.4 kV m^{-1}) were measured from the ER-2 over the massive cell around 2318 UTC (leg 3), suggesting multiple lightning discharges (Bateman et al. 1999). Such changes were much smaller over the same cell around 2331 UTC. The minimum 89 GHz T_b had increased considerably (lower right panel in Fig. 11), and a new burst was apparent to the northwest, along the Cordillera Central. It appears then that this convection was intense yet short-lived, and a spreading anvil did not form.

A similar development took place about 25 km to the southeast of this convective cell, about 30 min earlier. The 2245 UTC IR imagery revealed a convective tower with T_b of −72°C in that location, also over the Cordillera mountain range. Again the coldest top is displaced slightly to the east from the mountain crest. At 2315 UTC the coldest pixel, −73°C, coincided with the convective tower of Fig. 10, and it marks the last occurrence of very cold cloud tops in the eye in Fig. 3c. At 2345 UTC the coldest tops were −68°C and they were displaced ~30 km to the northwest. In short, *GOES-8* and MIR imagery suggest a sequence of intense convection travelling along the Cordillera Central.

7. Discussion

The eye of a mature hurricane contains anomalously warm, dry air as a result of subsident motion in the middle and upper troposphere, above one or more subsidence inversions at lower levels (Willoughby 1998). One may wonder how such an environment can support penetrating convection, as observed in Georges over the DR. It appears that even before landfall Georges's eye contained a large amount of convective available potential energy (CAPE): a dropsonde was released in the eye from the DC-8 at 10-km altitude on 21 September at 1823 UTC. Spontaneous parcel ascent in the eye at this time would have been inhibited by a subsidence inversion at 650 hPa, but an undiluted parcel lifted from the surface would become positively buoyant above 550 hPa, and at 10 km the parcel buoyancy would be as much as 9 K. The convective inhibition was about 80 J kg^{-1} in this sounding. Willoughby (1998) presented evidence that indicates that the dry air above the eye's subsidence inversion has a long residence time and that the airmass within the eye remains substantially the same during 24 h. The convective inhibition present in the 21 September eye sounding could have been eroded readily by frictional convergence after landfall and by forced ascent over the steep topography of Hispaniola. Two station observations within the eye offer some evidence for ascent within the eye after landfall. Sabana Perdida in the southeastern lowlands of the DR (location shown in Fig. 1) was close to the center of the eye at 1745 UTC. At that time the barograph reading at Sabana dipped to 973 hPa (adjusted to sea level), 24 hPa higher than the minimum SLP registered 55 min earlier at Bayaguana on the coast. The pressure readings at these two stations appear to have been reasonably accurate, and the eye's center appears to have passed both stations within 5–10 km. Therefore these data indicate a rapid filling of the cyclone, which suggests rising motion in the eye. Ascent may occur at any level but is particularly effective in increasing surface pressure hydrostatically if it occurs in a stable layer, because of the large cooling it implies, that is, near the subsidence inversion and/or near the tropopause. The IR brightness temperatures generally increased in the eyewall, especially during landfall (1500–1800 UTC), making ascent in the tropopause region unlikely. Ascent starting at low levels is more likely: in fact, convection within the eye started during this period of rapid pressure increase, around 1715 UTC.

The forcing at the surface, combined with instability aloft, resulted in deep and overshooting convection within the eye, eventually entirely filling the eye. The most intense convection coincided with the main mountain range, and it traveled as a sequence of cells along the mountain range in the direction of the hurricane motion. One may wonder why this sequence of overshooting cells was so short-lived. The likely answer is that the two key forcing factors were short-lived as well. First, forced ascent over topography is conditional upon the low-level wind pattern, which changed rapidly in response to the movement of the eye. Second, the CAPE locked in the eye was released rapidly and not replenished by surface heat fluxes because of the hurricane's location over land. Surface sensible and latent heat fluxes in hurricanes over water normally are largest just outside the eyewall, where the wind-induced heat fluxes are large enough to compensate for air with lower θ_e carried into the boundary layer by convective downdrafts (Willoughby 1990). When deep convection breaks out in or near Georges's eye over land, surface heat fluxes are relatively small and a convectively stabilized boundary layer forms. Low-level moisture convergence into the cyclone continues, but the surface becomes increasingly decoupled and the precipitation more stratiform. In short, we believe that the deep convection in the eye was the result of localized and short-lived orographic forcing, which tapped preexisting CAPE. Deep convection within the eye depletes the limited supply of CAPE and produces a more stable temperature profile. Weakening of a hurricane without penetrating eye convection is associated with reduced subsidence and therefore a less stable profile. One outstanding question that follows from these opposing effects is how deep eye convection affects the overall storm dynamics. Thermal wind balance suggests that eye convection further weakens the primary hurricane circulation, primarily near the level of free convection (about 5 km in this case).

The topography also affected the low-level reflectivity profiles: fall streak curvatures and EDOP forward-beam velocity data indicate that the low-level horizontal airflow is confluent around the eye in all three sections shown here. This low-level convergence, combined with upslope flow toward the Cordillera Central, implies strong low-level ascent. Such ascent supports a large concentration of cloud water. This in turn enhances rain formation at low levels. In fact, the EDOP radar reflectivity increases from the minimum below the bright band to the ground by an average of 0.6 dB km^{-1} in all onshore stratiform rainbelts in legs 1–3 (Fig. 9c). This low-level rainfall enhancement cannot be detected by spaceborne passive microwave or infrared sensors, nor can it be seen by ground-based scanning radars in mountainous terrain (e.g., Fig. 5). A lapse rate of 0.6 dB km^{-1} implies a cloud-water content of 0.7 g kg^{-1}, assuming a Marshall–Palmer drop size distribution, a median drop diameter of 2 mm (Ulbrich et al. 1999), growth by collection only, and a collection of efficiency of 1.0. Such cloud-water content is moderately high compared to some in situ observations in hurricanes (Black and Hallett 1986). A downward increase of reflectivity below the bright band is not observed in the rainband just south of Hispaniola (leg 2, Fig. 9a). The difference is probably due to the low-level ascent onshore, over sloping terrain or along sloping θ_e lines. Close-ups of parts of the cross sections shown in this paper reveal a clear correlation between local terrain slope and vertical motion: horizontal flow over hills and mountains triggers ascent. Most of these currents of rising air remain shallow, suggesting that they are either tilted or not buoyant. Whether the convection is forced or free, the shallow rising currents leave an imprint on the reflectivity field. It is these local currents that may be responsible for the observed net reflectivity lapse rate.

However, cloud microphysical factors cannot be excluded in the explanation of the reflectivity lapse rate. An increase in reflectivity can be due to an increase in median drop diameter, without change in rain mixing ratio or rain rate. Reflectivity may be enhanced by collision–coalescence, which may be more effective over land because continental clouds typically have more cloud condensation nuclei (Twohy and Hudson 1995) and therefore more droplets. In marine clouds, the median drop size diameter tends to be larger. Therefore the break up of large drops is more likely in the offshore rainband, and this reflectivity reducing process may offset the growth of smaller drops by condensation–coalescence. In other words, low-level rainfall enhancement may be equally present in the offshore rainband, but it may not be apparent in the reflectivity profile. However, the continental–marine separation, in particular the classification of Georges's precipitation over the island of Hispaniola as continental, is questionable.

The EDOP and passive microwave observations such as over Georges complement existing observational capabilities of the NOAA HRD aircraft. These observations are useful to improve quantitative rain-

fall prediction in landfalling hurricanes. For instance, convective eruptions of the kind described here, superimposed on widespread enhanced stratiform rain, may have been responsible for several mudslides and flash floods that resulted in many casualties on Hispaniola. Similar convective events, and associated hazards, may have occurred in the mountains of Central America in late October 1998 on account of Hurricane Mitch, one of the deadliest Atlantic tropical cyclones in history. Several places in Honduras and Nicaragua[3] reported daily rainfall totals over 200 mm after Mitch, a category 5 storm on 26 October, had moved onshore and had weakened to a tropical storm. Satellite estimates also suggest that most rain fell *after* Mitch's decay to tropical storm status, especially near Nicaragua's west coast (Ferraro et al. 1999). Apparently even weak tropical disturbances can continue to converge large amounts of water vapor after landfall, especially when the land area is surrounded by warm seas. The evolution of low-level convergence of air and moisture during Georges's landfall over Hispaniola is a focus of ongoing work, which uses EDOP-derived along-track winds and dropsonde data. Hispaniola was relatively fortunate in that Georges, in comparison to Mitch, moved fairly rapidly over the island.

8. Conclusions

On 22 September 1998 Hurricane Georges made landfall on the mountainous island of Hispaniola. Georges dumped up to 500 mm of rain on the island, making it one of the worst natural disasters of Hispaniola. The NASA ER-2 flew over this landfalling hurricane with several remote sensors including EDOP, an X-band nadir and forward viewing Doppler radar. For the first time ever, high-resolution reflectivity and along-track airflow data were collected over a hurricane interacting with complex topography. In particular, EDOP witnessed the development and collapse of a massive convective event over the Cordillera Central mountain range.

In several respects Georges weakened as it made landfall. The minimum sea level pressure increased about 23 hPa in a period estimated between 1 and 9 h. The maximum sustained wind declined, the eye (as seen in visible and infrared satellite imagery) filled in, the upper-level warm anomaly weakened, and the satellite IR and 85.5-GHz brightness temperatures generally increased in the eyewall. All these changes, except the eyewall brightness temperatures and perhaps the minimum SLP, were most rapid not at the time of landfall on the plains of southeastern Hispaniola, but rather between 2 and 5 h after landfall, when the eye moved over the mountains. During the period of rapid change, the aircraft-estimated 89-GHz brightness temperature also increased in the eyewall. On the Saffir–Simpson scale, Georges weakened from a category 3 to a category 1 hurricane in less than 6 h.

Yet there are signs that upon landfall Georges became more intense, at least temporarily and locally, in terms of convective activity and surface rainfall. Geostationary satellite, ground-based radar, EDOP, and ER-2 passive microwave imagery suggest that when Georges moved over Hispaniola, convection broke out within the eye, in several pulses. The eye, as seen from space, was filled by a convective anvil first, before it was filled by hydrometeors at all levels. Two overshooting convective events within the eye were documented. The second one featured updrafts over 20 m s^{-1}, 35 dBZ echoes above a height of 12 km, and upwelling 89-GHz radiation corresponding to a T_b less than 100 K. The location, intensity, and evolution of this convection indicate that it was coupled to the surface orography. Convection of such intensity is consistent with the high CAPE value measured in a sounding through the eye on the previous day. We speculate that this energy was trapped under a weak subsidence inversion, which was eroded as the eye was lifted over Hispaniola's topography.

EDOP-derived vertical profiles over land show an increase in reflectivity of 0–2 dBZ km^{-1} from the minimum below the bright band to the surface, whereas a decrease occurs over the same depth in an offshore rainband. This low-level rain enhancement, which cannot be detected by ground radars in complex terrain, nor by satellite measurements of upwelling infrared or microwave radiation, is believed to be due to the ascent of boundary layer air over the topography or over sloping surfaces of constant moist static energy.

Acknowledgments. This work was supported by NASA TRMM, USWRP, and CAMEX-3 programs managed by Dr. Ramesh Kakar at NASA Headquarters. The CAMEX-3 program was part of a multiagency (NASA, NOAA, and NSF) effort to study hurricanes. Many thanks go to all the people involved in providing the facilities and logistics to make this experiment pos-

[3]According to NHC's preliminary report on Hurricane Mitch, available online at http://www.nhc.noaa.gov/1998mitch.html.

sible. Particular thanks go to Robbie Hood, Ed Zipser, and Ed Bensman, who coordinated the ER-2 flight over Georges. The rain gauge data and Santo Domingo radar images were provided by the Oficina Nacional de Meteorologia de la Republica Dominicana. MIR data and their interpretation were provided by James Wang. Ye Hong, Hal Pierce, and Eric Nelkin assisted with the SSM/I and TMI data. Much insight was gained from discussions with Joanne Simpson, Dalin Zhang, Arlene Laing, Richard Blakeslee, Ed Rodgers, and Dee Porter, the ER-2 pilot on this flight.

References

Bateman, M. G., R. J. Blakeslee, J. C. Bailey, M. F. Stewart, and A. K. Blair, 1999: High-altitude aircraft-based electric field measurements above thunderstorms. Preprints, *11th Int. Conf. on Atmos. Electr.,* Guntersville, AL, International Conference on Atmospheric Electricity, National Aeronautics and Space Administration, National Science Foundation, 527–529.

Bender, M. A., R. E. Tuleya, and Y. Kurihara, 1987: A numerical study of the effect of island terrain on tropical cyclones. *Mon. Wea. Rev.,* **115,** 130–155.

Black, M. L., and H. E. Willoughby, 1992: The concentric eyewall cycle of Hurricane Gilbert. *Mon. Wea. Rev.,* **120,** 947–957.

——, R. W. Burpee, and F. D. Marks Jr., 1996: Vertical motion characteristics of tropical cyclones determined with airborne Doppler radial velocities. *J. Atmos. Sci.,* **53,** 1887–1909.

Black, R. A., and J. Hallett, 1986: Observations of the distribution of ice in hurricanes. *J. Atmos. Sci.,* **43,** 802–822.

Blackwell, K. G., 2000: The evolution of Hurricane Danny (1997) at landfall: Doppler-observed eyewall replacement, vortex contraction/intensification, and low-level wind maxima. *Mon. Wea. Rev.,* in press.

Dodge, P., R. W. Burpee, and F. D. Marks Jr., 1999a: The kinematic structure of a hurricane with sea level pressure less than 900 mb. *Mon. Wea. Rev.,* **127,** 987–1004.

——, S. Houston, W. Lee, J. Gamache, and F. D. Marks, Jr., 1999b: Windfields in Hurricane Danny (1997) at landfall from combined WSR-88D and airborne Doppler radar data. Preprints, *23d Conf. on Hurricanes and Tropical Meteorology,* Dallas, TX, Amer. Meteor. Soc., 61–62.

Emanuel, K. A., 1986: An air–sea interaction theory for tropical cyclones. Part I: Steady-state maintenance. *J. Atmos. Sci.,* **43,** 585–604.

Ferraro, R., G. Vicente, M. Ba, A. Gruber, R. Scofield, Q. Li, and R. Weldon, 1999: Satellite techniques yield insight into devastating rainfall from Hurricane Mitch. *Eos, Trans. Amer. Geophys. Union,* **80,** 505–514.

Halverson, J. B., H. Pierce, J. Simpson, C. Morales, and E. Rodgers, 1999: First TRMM satellite observations of a deep convective burst in supertyphoon Paka (1997). Preprints, *23d Conf. on Hurricanes and Tropical Meteorology,* Dallas, TX, Amer. Meteor. Soc., 997–1000.

Heymsfield, G. M., and R. Fulton, 1988: Comparison of high-altitude remote aircraft measurements with the radar structure of an Oklahoma thunderstorm: Implications for precipitation estimation from space. *Mon. Wea. Rev.,* **116,** 1157–1174.

——, S. Bidwell, I. J. Caylor, S. Ameen, S. Nicholson, W. Boncyk, L. Miller, D. Vandemark, P. E. Racette, and L. R. Dod, 1996a: The EDOP radar system on the high-altitude NASA ER-2 aircraft. *J. Atmos. Oceanic Technol.,* **13,** 795–809.

——, I. J. Caylor, J. M. Shepherd, W. S. Olson, S. Bidwell, W. Boncyk, and S. Ameen, 1996b: Structure of Florida thunderstorms using high-altitude aircraft radiometer and radar observations. *J. Appl. Meteor.,* **35,** 1736–1762.

——, B. Geerts, and L. Tian, 2000: TRMM precipitation radar reflectivity profiles compared to high-resolution airborne and ground-based measurements. *J. Appl. Meteor.,* submitted.

Houze, R. A., Jr., 1993: *Cloud Dynamics.* Academic Press, 573 pp.

Jorgensen, D. P., E. J. Zipser, and M. A. LeMone, 1985: Vertical motions in intense hurricanes. *J. Atmos. Sci.,* **42,** 839–856.

Kong, K., and J. B. Elsner, 1999: Baroclinic structure of Hurricane Danny at landfall. Preprints, *23d Conf. on Hurricanes and Tropical Meteorology,* Dallas, TX, Amer. Meteor. Soc., 63–65.

Kummerow, C., and L. Giglio, 1994: A passive microwave technique for estimating rainfall and vertical structure information from space. Part II: Applications to SSM/I data. *J. Appl. Meteor.,* **33,** 19–34.

Lee, C., and G. Jian, 1999: A numerical simulation of a landfalling typhoon in Taiwan. Preprints, *23d Conf. on Hurricanes and Tropical Meteorology,* Dallas, TX, Amer. Meteor. Soc., 78–79.

Li, J., N. E. Davidson, G. D. Hess, and G. Mills, 1997: A high-resolution prediction study of two typhoons at landfall. *Mon. Wea. Rev.,* **125,** 2856–2878.

Marks, F. D., and R. A. Houze, 1987: Inner core structure of Hurricane Alicia from airborne Doppler radar observations. *J. Atmos. Sci.,* **44,** 1296–1317.

——, L. K. Shay, and Coauthors, 1998: Landfalling tropical cyclones: forecast problems and associated research opportunities. *Bull. Amer. Meteor. Soc.,* **79,** 305–323.

McCaul, E. W., and M. L. Weisman, 1996: Simulations of shallow supercell storms in landfalling hurricane environments. *Mon. Wea. Rev.,* **124,** 408–429.

Mejia, M. I., and L. P. Rodriguez, 1999: Georges: 15–27 September 1998, 24 pp. [Available from the Oficina Nacional de Meteorologia, Santa Domingo, Dominican Republic.]

Mohr, K. I., E. R. Toracinta, E. J. Zipser, and R. E. Orville, 1996: A comparison of WSR-88D reflectivities, SSM/I brightness temperatures, and lightning for mesoscale convective systems in Texas. *J. Appl. Meteor.,* **35,** 919–931.

Powell, M. D., and S. H. Houston, 1998: Surface wind fields of 1995 hurricanes Erin, Opal, Luis, Marilyn and Roxanne at landfall. *Mon. Wea. Rev.,* **126,** 1259–1273.

Riehl, H., and J. S. Malkus, 1961: Some aspects of Hurricane Daisy. *Tellus,* **13,** 181–213.

Riordan, A. J., and J. Cline, 1999: Inland re-intensification of tropical storm Danny. Preprints, *23d Conf. on Hurricanes and Tropical Meteorology,* Dallas, TX, Amer. Meteor. Soc., 1016–1019.

Shapiro, L. J., and H. E. Willoughby, 1982: The response of balanced hurricanes to local sources of heat and momentum. *J. Atmos. Sci.,* **39,** 378–394.

Simpson, J., B. Ferrier, R. Simpson, J. Halverson, W. Peterson, R. Blakeslee, and S. Durden, 1998: On the role of "hot towers" in tropical cyclone formation. *Meteor. Atmos. Phys.,* **67,** 15–35.

Spencer, R. W., H. M. Goodman, and R. E. Hood, 1989: Precipitation retrieval over land and ocean with the SSM/I: Identification and characteristics of the scattering signal. *J. Atmos. Oceanic Technol.,* **6,** 254–273.

Stewart, R. E., J. D. Marwitz, J. C. Pace, and R. E. Carbone, 1984: Characteristics through the melting layer of stratiform clouds. *J. Atmos. Sci.,* **41,** 3227–3237.

Stewart, S. R., J. Simpson, and D. Wolff, 1997: Convectively induced mesocyclonic vortices in the eyewall of tropical cyclones as seen by WSR-88D Doppler radars. Preprints, *22d Conf. on Hurricanes and Tropical Meteorology,* Fort Collins, CO, Amer. Meteor. Soc., 105–108.

Twohy, C. H., and J. G. Hudson, 1995: Measurements of cloud condensation nuclei spectra within maritime cumulus cloud droplets—Implications for mixing processes. *J. Appl. Meteor.,* **34,** 815–833.

Ulbrich, C. W., M. Petitdidier, and E. F. Campos, 1999: Radar properties of tropical rain found from disdrometer data at Arecibo, Puerto Rico. Preprints, *29th Conf. on Radar Meteorology,* Montreal, PQ, Canada, Amer. Meteor. Soc., 676–679.

Wang, T. C., and C. H. Tseng, 1999: The structure of Typhoon Herb (1996) during its landfall by dual Doppler analysis. Preprints, *29th Conf. on Radar Meteorology,* Montreal, PQ, Canada, Amer. Meteor. Soc., 364–365.

Willis, P. T., and A. J. Heymsfield, 1989: Structure of the melting layer in mesoscale convective system stratiform precipitation. *J. Atmos. Sci.,* **46,** 2008–2025.

Willoughby, H. E., 1990: Temporal changes of the primary circulation in tropical cyclones. *J. Atmos. Sci.,* **47,** 242–264.

——, 1998: Tropical cyclone eye thermodynamics. *Mon. Wea. Rev.,* **126,** 3053–3067.

——, and P. G. Black, 1996: Hurricane Andrew in Florida: dynamics of a disaster. *Bull. Amer. Meteor. Soc.,* **77,** 543–549.

——, J. A. Clos, and M. G. Shoreibah, 1982: Concentric eye walls, secondary wind maxima, and the evolution of the hurricane vortex. *J. Atmos. Sci.,* **39,** 395–411.

Wu, C. C., and Y. H. Kuo, 1999: Typhoons affecting Taiwan: Current understanding and future challenges. *Bull. Amer. Meteor. Soc.,* **80,** 67–80.

Yuter, S. E., and R. A. Houze Jr., 1995: Three-dimensional kinematic and microphysical evolution of Florida cumulonimbus. Part II: Frequency distributions of vertical velocity, reflectivity, and differential reflectivity. *Mon. Wea. Rev.,* **123,** 1941–1963.